Research Article

David Bogensberger, Fraser Clarke, and Anthony Eugene Lynas-Gray*

Further Evidence of a Brown Dwarf Orbiting the Post-Common Envelope Eclipsing Binary V470 Cam (HS 0705+6700)

https://doi.org/10.1515/astro-2017-0015
Received Aug 18, 2017; accepted Oct 13, 2017

Abstract: Several post-common envelope binaries have slightly increasing, decreasing or oscillating orbital periods. One of several possible explanations is light travel-time changes, caused by the binary centre-of-mass being perturbed by the gravitational pull of a third body. Further studies are necessary because it is not clear how a third body could have survived subdwarf progenitor mass-loss at the tip of the Red Giant Branch, or formed subsequently. Thirty-nine primary eclipse times for V470 Cam were secured with the Philip Wetton Telescope during the period 2016 November 25th to 2017 January 27th. Available eclipse timings suggest a brown dwarf tertiary having a mass of at least 0.0236(40) $M_{\odot}$, an elliptical orbit with an eccentricity of 0.376(98) and an orbital period of 11.77(67) years about the binary centre-of-mass. The mass and orbit suggest a hybrid formation, in which some ejected material from the subdwarf progenitor was accreted on to a precursor tertiary component, although additional observations would be needed to confirm this interpretation and investigate other possible origins for the binary orbital period change.

Keywords: stars: subdwarfs, stars: binaries eclipsing, stars: binaries close

1 Introduction

Among the thirteen post-common envelope binaries (PCEBs) Zorotovic & Schreiber (2013) list as having a hot subdwarf, Lohr et al. (2014) identify nine HW Vir-type binaries bright enough to have archived SuperWASP (Pollacco et al. 2006) observations at a cadence suited to determinations of orbital period (Π) and its change rate ($\dot{\Pi}$). In the cases of AA Dor and NSVS 07826147, Lohr et al. confirm constant Π; for HS 2231+2441, 2M 1938+4603 and NSVS 07826147 they find upper limits for $\dot{\Pi}$ of 0.03, 0.01 and 0.0003 s yr^{-1} respectively. Only in the cases of HW Vir and ASAS J102322–3737 do Lohr et al. find $\dot{\Pi}$ to be greater than its detection threshold ($\dot{\Pi}_{\rm thresh}$), convincingly suggesting $|\dot{\Pi}| > 0$, for the first time in the case of ASAS J102322–3737. Although Lohr et al. find $|\dot{\Pi}| > 0$ for the remaining objects (EC 10246–2707, NY Vir and NSVS 14256825), the result is not convincing since $|\dot{\Pi}| < \dot{\Pi}_{\rm thresh}$.

An advantage gained in using a facility like SuperWASP lies in homogeneity of the data analysed, though the sample of PCEBs observed is too small to provide robust statistics. Lohr et al. (2015) determine Π and $\dot{\Pi}$ for a general sample of 13927 eclipsing binaries using archived SuperWASP observations. Only in 2% of cases do Lohr et al. find Π to have a sinusoidal variation, suggesting third bodies in those systems; in 22% of cases they find Π to vary linearly and argue that this could be indicative of a longer-term sinusoidal Π variation caused by third bodies in systems. Taking the two numbers together, Lohr et al. propose a multiplicity of three or more for 24% of SuperWASP binaries, in good agreement with earlier determinations (Duchêne & Kraus 2013) for the fraction of multiple systems among binaries in general.

PCEB eclipse time variations are frequently (for example by Lee et al. 2009) interpreted as light travel-time changes, due to reflex motion of the binary centre-of-mass as a consequence of one or more orbiting bodies. But measurements of $\dot{\Pi}$ for PCEBs obtained over a time interval of the same order as a proposed Π can only tentatively identify an orbiting planet, brown dwarf or M dwarf. Further comments are given by Kilkenny (2014).

Corresponding Author: Anthony Eugene Lynas-Gray: Department of Physics, University of Oxford, United Kingdom, E-mail: aelg@astro.ox.ac.uk
David Bogensberger: Department of Physics, University of Oxford, United Kingdom, E-mail: david.bogensberger@lmh.ox.ac.uk
Fraser Clarke: Department of Physics, University of Oxford, United Kingdom, E-mail: Fraser.Clarke@physics.ox.ac.uk

Applegate (1992) proposes an alternative explanation for eclipse timing variations as a gravitational coupling of a binary orbit to changes in the shape of a magnetically active star in the system. However, Völschow et al. (2016) conclude that an improved version of the "Applegate mechanism", which includes angular momentum exchange between a finite shell and the stellar core, cannot uniquely explain Π variations in the sixteen systems they consider. Zorotovic & Schreiber (2013) argue for additional observations to distinguish between the "Applegate mechanism" and post-common envelope planet formation. Kostov et al. (2016) and Veras et al. (2017) show that planets could survive a common envelope ejection, though distinguishing these from planets formed afterwards would require new techniques.

Resonant interactions between PCEBs and circumbinary disks could also explain $\left|\dot{\Pi}\right| > \dot{\Pi}_{\rm thresh}$. Calculations by Chen & Podsiadlowski (2017) suggest a circumbinary disk having a mass in the range $10^{-4}\,{\rm M}_{\odot} - 10^{-2}\,{\rm M}_{\odot}$ would explain $\dot{\Pi}$ observations for HW Vir and NY Vir, where one PCEB component is a hot subdwarf. Chen & Podsiadlowski note the detection of a circumbinary disk around NN Ser, and argue for more extensive searches for them around other PCEBs.

Drechsel et al. (2001) identify V470 Cam (HS 0705+6700) as a PCEB. Subsequent times of primary minimum (Niarchos et al. 2003; Németh et al. 2005; Kruspe et al. 2007; Qian et al. 2009) show departures from the Drechsel et al. (2001) linear ephemeris, which Qian et al. (2009) attribute to a circumbinary low-luminosity object. Further eclipse timings (Beuermann et al. 2012; Qian et al. 2013; Pulley et al. 2015) provide improved estimates for the proposed tertiary component orbital parameters. As V470 Cam is well-placed for observing $\left[\alpha(2000) = 07^{\rm h}10^{\rm m}42.07^{\rm s}, \delta(2000) = +67^{\rm o}00^{'}43.6^{"}\right]$ during a Northern Hemisphere winter, and bright enough ($B = 14.1$) to observe with a small telescope at a city-centre site, we obtained additional light-curves and times of primary eclipse discussed in this paper.

2 Observations and Data Reduction

Over 6000 images centred on V470 Cam were obtained with the Philip Wetton Telescope (PWT) on nineteen nights between 2016 November 25$^{\rm th}$ and 2017 January 27$^{\rm th}$. A Johnson-V filter was used, and an exposure time of 60-s was adopted. Two to three primary eclipses were observed in a typical night. Data reduction was carried out with the Image Reduction and Analysis Facility in the usual way, applying bias and dark corrections to science and twilight flat-fields using the CCDRED package. Science frames were then corrected for pixel-to-pixel variation using normalised flat-fields. Magnitudes for V470 Cam and the adopted comparison star GSC22 0710387+665708 were measured in circular apertures using the DAOPHOT package, corresponding sky contributions being obtained from concentric annuli.

3 Results

Figure 1 shows the light-curve obtained for V470 Cam by phasing all differentially corrected magnitudes using Dworetsky's (1983) string-length method. As is standard practice, a phase $\phi = 0$ was adopted at primary minimum. A fit to the magnitude (m) in primary eclipse, shown as a red line in Figure 1, was obtained using

$$m = a \exp\left(-\left|\frac{\phi}{w}\right|^{p}\right) + M_0 + r\,|\phi|\,, \qquad (1)$$

an adaptation of the Beuermann et al. (2012) fitting function. Values obtained for fit parameters are listed in Table 1 where a is the primary eclipse depth, M_0 the magnitude at

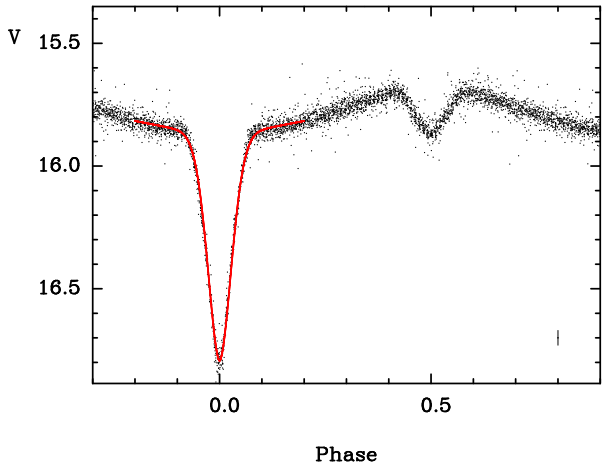

Figure 1. PWT Light-Curve for V470 Cam, the typical error in each observation being plotted in the bottom right hand corner.

Table 1. Primary Eclipse Fit Parameters

Parameter	Value (error)	Units
a	+0.9098(45)	magnitudes
w	+0.03969(15)	cycles
p	+1.822(17)	
M_0	15.8834(22)	magnitudes
r	−0.335(12)	magnitudes/cycle

$\phi = 0$ if there were no eclipse, w the primary eclipse width and r the reflection effect gradient.

Individual light-curves were cross-correlated with the combined Figure 1 light-curve to give, using the Equation 1 fit to its primary eclipse, Barycentric Julian dates (BJD) of primary minima listed in the second column of Table 2. For a light-curve based on thousands of magnitude measurements made within a short time interval, cross-correlation seemed to be superior to the commonly used Kwee & van Woerden (1956) method. Mikulášek et al. (2014) argue that the Kwee & van Woerden method yields accurate times of minima, but underestimates errors. The cross-correlation method compares entire light-curves, and does not require symmetry about minima.

Running eclipse numbers (N), listed in the left-hand column of Table 2, were based on the Drechsel et al. (2001) ephemeris; our ephemeris

$$T = 2451822.75857(24) + 0.0956466934(38)N \quad (2)$$

then followed from a linear least squares fit. Although the period agreed with the Drechsel et al. period within formal least squares error limits, epochs differ (in the sense Drechsel et al. – this paper) by 0.00198(24) days, which was interpreted as a consequence of known period changes. Errors in primary eclipse times evaluated by fitting Equation 1, and perturbing the cross-correlation determination, were 0.000096 days. Differences between observed (Table 2 – Column 2) and calculated (Drechsel et al. 2001) times of primary eclipse ($O - C$) are listed in the right-hand column of Table 2 and included with literature values in Figure 2.

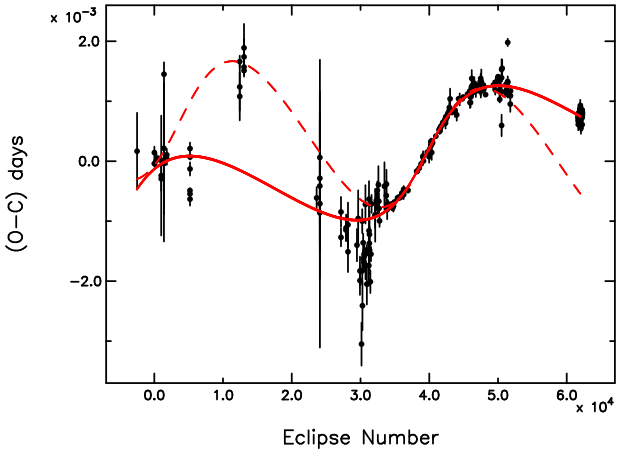

Figure 2. Departures (O-C) of Observed (2000-2017) Times of Primary Eclipse from those Predicted using the Drechsel et al. Linear Ephemeris

Table 2. Times of Primary Eclipse

N	Minima BJD – 2400000	(O-C) days
61672	57721.481516	0.000769
61673	57721.577119	0.000724
61674	57721.672654	0.000612
61682	57722.437879	0.000665
61684	57722.629252	0.000744
61685	57722.724840	0.000685
61692	57723.394425	0.000745
61693	57723.490131	0.000803
61694	57723.585680	0.000706
61725	57726.550737	0.000717
61726	57726.646344	0.000677
61734	57727.411578	0.000738
61922	57745.393271	0.000860
61925	57745.680067	0.000717
61934	57746.541046	0.000876
61963	57749.314688	0.000765
61964	57749.410281	0.000712
61966	57749.601790	0.000927
61967	57749.697261	0.000751
61984	57751.323335	0.000832
61985	57751.418926	0.000777
61988	57751.705898	0.000809
62036	57756.296792	0.000664
62037	57756.392371	0.000595
62038	57756.488182	0.000760
62059	57758.496719	0.000717
62060	57758.592353	0.000705
62061	57758.688089	0.000794
62069	57759.453021	0.000553
62070	57759.548896	0.000782
62235	57775.330641	0.000829
62236	57775.426183	0.000725
62237	57775.521959	0.000854
62245	57776.287125	0.000847
62246	57776.382673	0.000748
62247	57776.478182	0.000610
62266	57778.295679	0.000822
62267	57778.391275	0.000771
62289	57780.495527	0.000796

With one notable exception, our subsequent analysis included all available times of primary eclipse from Table 2 and literature sources listed above. We retained the two eclipse timings Qian et al. (2009) discard. The exception was the eclipse $N = 30149$, not plotted in Figure 2, as $(O - C) = -0.0057$ days. The absolute value of $(O - C)$ for $N = 30149$ is 2.1 times larger than the maximum for an included eclipse timing (for $N = 30150$), but is an order of magnitude larger than typical values. Our replication of fits by Qian et al. (2009) and Qian et al. (2013) suggested that these authors also discard the $N = 30149$ eclipse, al-

though we did not find this to be explicitly stated in either paper.

We followed Qian et al. (2013, their equations 2-5) by assuming $(O-C)$ variations in Figure 2 to be attributable to a third body in the system and determined its orbital parameters using Kepler's Equation, expressing $(O-C)$ in terms of the eccentric anomaly (E) and iteratively solving the resulting equation:

$$(O-C) = \Delta T_0 + N\Delta P_0 + A\left(\sqrt{1-e^2}\sin E\cos\omega + \cos E\sin\omega\right). \quad (3)$$

The derived fit is the red curve shown in Figure 2; the corresponding third-body orbital parameters listed in Table 3 were: ΔT_0 – epoch correction, ΔP_0 – period correction, A – amplitude of oscillation, e – orbital eccentricity, ω – longitude of periastron passage, Π_3 – orbital period and τ – time of periastron passage. For comparison, the Qian et al. fit was plotted in Figure 2 as a red dashed curve and the corresponding orbital parameters included in Table 3 as the second column; it predicts $(O-C) \sim -47(17)$-s at the epoch of our observations whereas we obtained a mean of 64.60(13)-s from our fit, forcing a sign change in ΔT_0 and ΔP_0 (see Qian et al., their equation 3) and hence the appearance of a positive gradient in our fit plotted in Figure 2.

Table 3. Third Object Orbital Parameters

Parameter	Qian et al. (2013)	This Paper
ΔT_0 (days)	$+7.23(65) \times 10^{-4}$	$-8.93(47) \times 10^{-4}$
ΔP_0 (days)	$-1.24(17) \times 10^{-8}$	$+2.61(11) \times 10^{-8}$
A (seconds)	96.2(10)	81.7(11)
e	0.22(2)	0.376(98)
ω (degrees)	$3.529(57) \times 10^2$	$3.578(11) \times 10^2$
Π_3 (years)	9.53(10)	11.77(67)
τ (BJD)	2452127(68)	2451296(22)

4 Conclusion

Niarchos et al. (2003) obtain $M_1 = 0.49(15)\,M_\odot$ and $M_2 = 0.13(5)\,M_\odot$ as masses for the V470 Cam eclipsing binary components; from these and orbital parameters for the tertiary component presented in Table 3, its mass was determined to be $M_3 \sin i = 0.0236(40)\,M_\odot$, where i is the orbital inclination. It would therefore appear that any tertiary component would have to be a brown dwarf if it were to account for observed binary period changes. The obvious disparity between the two fits in Figure 2 demonstrated the crucial importance of long-term monitoring to obtain an improved understanding of PCEB eclipse time variations, as well as allowing for an analysis of possible second-order effects.

Another issue is the deduced Π_3 in Table 3 which is more than half the time-interval ($\sim$16.97 years) over which primary eclipse times have been obtained; fewer than two orbits of the suggested third-body have been observed and at least another decade of primary eclipse time measurements would be needed to clarify the origin of $(O-C)$ variations plotted in in Figure 2. An analysis by Sahlmann et al. (2015) suggests an astrometric detection of the V470 Cam hot subdwarf reflex motion, due to its eclipsing companion, will be made by GAIA. If so, a tertiary would also be astrometricaly detectable over the proposed lifetime of the GAIA mission.

The existence of a few PCEBs in which the secondary is a brown dwarf (Schaffenroth et al. 2015) suggests that these not only survive a common envelope phase of evolution but play an essential role in triggering it. In the case of V470 Cam, for a brown dwarf tertiary component to have survived a common envelope phase would have required an even larger orbital eccentricity and semi-major axis, as Schleicher et al. (2015) explain. A second formation hypothesis suggests a tertiary would have formed from the ejected envelope, but it is not clear that a brown dwarf could form in this way with an orbital eccentricity of 0.376(98). A further possibility which Schleicher et al. propose is a hybrid hypothesis in which a low-mass precursor is driven into an eccentric orbit by envelope ejection and accretes material from it. Such a hybrid tertiary body could be expected to accrete the mass of a brown dwarf and obtain, after envelope ejection, an orbital eccentricity in between that of a newly formed and surviving brown dwarf.

Note Added in Proof: After the present paper was accepted for publication, we became aware of a more extensive study by Pulley et al. which appears to qualitatively confirm our (O-C) measurements for V470 Cam.

Acknowledgment: One of us (DB) is indebted to his family for financial support, and Lady Margaret Hall (University of Oxford) for a scholarship. Work presented in this paper was carried out with facilities provided by the University of Oxford, which also funded AEL-G's attendance at the Eighth Meeting on Hot Subdwarfs and Related Objects. The authors are indebted to an anonymous referee for helpful and constructive comments.

References

Applegate, J. H. 1992, ApJ, 385, 621-629.
Beuermann, K, Breitenstein, P., Dębski, B., Diese, J., Dubovsky, P. A., Dreizler, S. et al. 2012, A&A, 540, A8
Chen, W.-C., & Podsiadlowski, Ph. 2017, ApJL, 837, L19
Drechsel, H., Heber, U., Napiwotzki, R., Østensen, R., Solheim, J.-E., Johannessen, F. et al. 2001, A&A, 379, 893-904.
Duchêne, G., & Kraus, A. 2013, ARA&A, 51, 269-310.
Dworetsky, M. M. 1983, MNRAS, 203, 917-924.
Kilkenny, D. 2014, MNRAS, 445(1), 4247-4251.
Kostov, V. B., Moore, K., Tamayo, D., Jayawardhana, R., Rinehart, S. A. 2016, ApJ, 832(2), 183.
Kruspe, R., Schuh, S., Traulsen, I. 2007, IBVS, 5796.
Kwee, K. K., & van Woerden, H. 1956, BAN, 12, 327-330.
Lee, J. W., Kim, S.-L., Kim, C.-H., Koch, R. H., Lee, C.-U., Kim, H.-I. et al. 2009, AJ, 137, 3181-3190.
Lohr, M. E., Norton, A. J., Payne, S. G., West, R. G., Wheatley, P. J. 2015, A&A, 578, A136.
Lohr, M. E., Norton, A. J., Anderson, D. R., Collier Cameron, A., Faedi, F., Haswell, C. A et al. 2014, A&A, 566, A128.
Mikulášek, Z., Chrastina, M., Liška, J.,Zejda, M., Janík, J., Zhu, L.-Y et al. 2014, Contributions of the Astronomical Observatory Skalnate Pleso, 43(3), 382-387.
Németh, P., Kiss, L. L., Sarneczky, K. 2005, IBVS, 5599
Niarchos, P. G., Gazeas, K. D., Manimanis, V. N. 2003, in Astronomical Society of the Pacific Conference Series, 292, Interplay of Periodic, Cyclic and Stochastic Variability in Selected Areas of the H-R Diagram, ed. C. Sterken, 129-132.
Pollacco, D. L., Skillen, I., Collier Cameron, A., Christian, D. J., Hellier, C., Irwin, J et al. 2006, PASP, 118(848), 1407-1418.
Pulley, D., Faillace, G., Smith, D., Owen, C. 2015, Journal of the British Astronomical Association, 125 (5), 284-296.
Pulley, D., Faillace, G., Smith, D., Watkins, A., von Harrach, S. 2017, A&A (in press), arxiv.org/abs/1711.03749.
Qian, S.-B., Zhu, L.-Y., Zola, S., Liao, W.-P., Liu, L., Li, L.-J. et al. 2009, ApJL, 695, L163.
Qian, S.-B., Shi, G., Zola, S., Koziel-Wierzbowska, D., Winiarski, M., Szymanski, T. et al. 2013, MNRAS, 436(2), 1408-1414.
Sahlmann, J., Triaud, A. H. M. J., Martin, D. V. 2015, MNRAS, 447(1), 287-297.
Schaffenroth, V., Barlow, B. N., Drechsel, H., & Dunlap, B. H. 2015, A&A, 576, A123.
Schleicher, D. R. G., Dreizler, S., Völschow, M., Banerjee, R., Hessman, F. V. 2015, AN, 336(5), 458-463.
Veras, D., Georgakarakos, N., Dobbs-Dixon, I., Gänsicke, B. T. 2017, MNRAS, 465(1), 1008-1022.
Völschow, M., Schleicher, D. R. G., Perdelwitz, V., Banerjee, R. 2016, A&A, 587, A34.
Zorotovic, M., & Schreiber, M. R. 2013, A&A, 549, A95.

Philip Wetton Telescope

The Philip Wetton Telescope (PWT) is a 40-cm Meade LX200 Schmidt-Cassegrain mounted on top of the University of Oxford's Denys Wilkinson Building. This places the PWT at a longitude of $01^{o}15^{'}34^{''}$ west, a latitude of $+51^{o}45^{'}35^{''}$ and an altitude of 91 metres above sea-level. The telescope operates at f/6.3, with a $18' \times 12'$ field of view on a SBIG ST-8 CCD camera equipped with Johnson BVR filters. The observatory is controlled through the ACP observatory control software from DC-3 dreams. Combined with weather monitoring equipment, this enables fully robotic operation and hence very efficient data gathering. Though hampered by light pollution, the site has decent seeing (typically $< 2^{''}$) and around 100 clear nights per year.